JOURNAL OF VIROLOGY, Jan. 2005, p. 696–704 Vol. 79, No. 2
0022-538X/05/$08.00+0 doi:10.1128/JVI.79.2.696–704.2005

A Complex Zinc Finger Controls the Enzymatic Activities of Nidovirus Helicases

Anja Seybert,[1]† Clara C. Posthuma,[2] Leonie C. van Dinten,[2]‡ Eric J. Snijder,[2] Alexander E. Gorbalenya,[2] and John Ziebuhr[1]*

Institute of Virology and Immunology, University of Würzburg, Würzburg, Germany,[1] and Molecular Virology Laboratory, Department of Medical Microbiology, Leiden University Medical Center, Leiden, The Netherlands[2]

Received 29 June 2004/Accepted 18 August 2004

Nidoviruses (*Coronaviridae*, *Arteriviridae*, and *Roniviridae*) encode a nonstructural protein, called nsp10 in arteriviruses and nsp13 in coronaviruses, that is comprised of a C-terminal superfamily 1 helicase domain and an N-terminal, putative zinc-binding domain (ZBD). Previously, mutations in the equine arteritis virus (EAV) nsp10 ZBD were shown to block arterivirus reproduction by disrupting RNA synthesis and possibly virion biogenesis. Here, we characterized the ATPase and helicase activities of bacterially expressed mutant forms of nsp10 and its human coronavirus 229E ortholog, nsp13, and correlated these in vitro activities with specific virus phenotypes. Replacement of conserved Cys or His residues with Ala proved to be more deleterious than Cys-for-His or His-for-Cys replacements. Furthermore, denaturation-renaturation experiments revealed that, during protein refolding, Zn^{2+} is essential for the rescue of the enzymatic activities of nidovirus helicases. Taken together, the data strongly support the zinc-binding function of the N-terminal domain of nidovirus helicases. nsp10 ATPase/helicase deficiency resulting from single-residue substitutions in the ZBD or deletion of the entire domain could not be complemented in *trans* by wild-type ZBD, suggesting a critical function of the ZBD in *cis*. Consistently, no viral RNA synthesis was detected after transfection of EAV full-length RNAs encoding ATPase/helicase-deficient nsp10 into susceptible cells. In contrast, diverse phenotypes were observed for mutants with enzymatically active nsp10, which in a number of cases correlated with the activities measured in vitro. Collectively, our data suggest that the ZBD is critically involved in nidovirus replication and transcription by modulating the enzymatic activities of the helicase domain and other, yet unknown, mechanisms.

Nidoviruses feature the most complex genetic organization among plus-strand RNA viruses. Their replicase genes encode an exceptionally large number of nonstructural protein domains (7, 27, 40) which mediate the key functions required for genomic RNA synthesis (replication) and subgenomic RNA (sgRNA) synthesis (transcription) (16, 31). The replicase gene is comprised of two open reading frames (ORFs), ORF1a and ORF1b. ORF1a encodes the replicative polyprotein 1a (pp1a), and ORFs 1a and 1b together encode pp1ab (40, 42). Expression of the ORF1b-encoded part of pp1ab requires a −1 ribosomal frameshift during translation, which occurs just upstream of the ORF1a stop codon (3). The backbone of the replicase polyproteins is formed by a series of conserved domains that are arranged in a unique, nidovirus-specific order (5, 7, 8, 27, 29, 40). Some of these domains are rare or absent in other RNA viruses (27, 40, 41).

The nidovirus structural proteins and a number of virus-specific accessory proteins are encoded by up to 12 ORFs located downstream of the replicase gene (11, 30, 32). These ORFs are expressed from a nested set of 3′-coterminal sgRNAs that, in coronaviruses and arteriviruses, possess a common 5′ leader sequence that is identical to the 5′ end of the genome. It is currently believed that these leader-containing sgRNAs are generated from subgenomic minus-strand templates that are produced by discontinuous RNA synthesis (19, 22, 23, 43).

The unique features of nidovirus RNA synthesis are undoubtedly linked with the viral proteome. Previous sequence analyses identified two nidovirus-wide conserved domains that are absent in other RNA viruses (7). One of these is comprised of about 80 to 100 residues, including 12 to 13 conserved Cys/His residues (8, 35). The domain forms the N-terminal part of a protein containing a superfamily 1 helicase domain in its C-terminal half (Fig. 1). Based on its primary structure, the Cys/His-rich segment was proposed to form a complex binuclear Zn-binding domain (ZBD) that may be involved in RNA synthesis (35). Point mutations in the ZBD or a protein segment called the hinge spacer, which is located immediately downstream of the ZBD's most C-terminal Cys residue, disrupted RNA synthesis in equine arteritis virus (EAV), the prototype arterivirus (35). Other mutations in this region selectively impaired sgRNA synthesis (34, 35).

The ZBD-containing protein is known as nonstructural protein 10 (nsp10) in EAV (36) and nsp13 (formerly $p66^{HEL}$) in human coronavirus 229E (HCoV-229E) (24, 40). Previously, it

* Corresponding author. Mailing address: Institute of Virology and Immunology, University of Würzburg, Versbacher Str. 7, 97078 Würzburg, Germany. Phone: 49-931-20149928. Fax: 49-931-20149553. E-mail: j.ziebuhr@mail.uni-wuerzburg.de.

† Present address: European Molecular Biology Laboratory, Heidelberg, Germany.

‡ Present address: Department of Immunohematology and Blood Transfusion, Leiden University Medical Center, Leiden, The Netherlands.

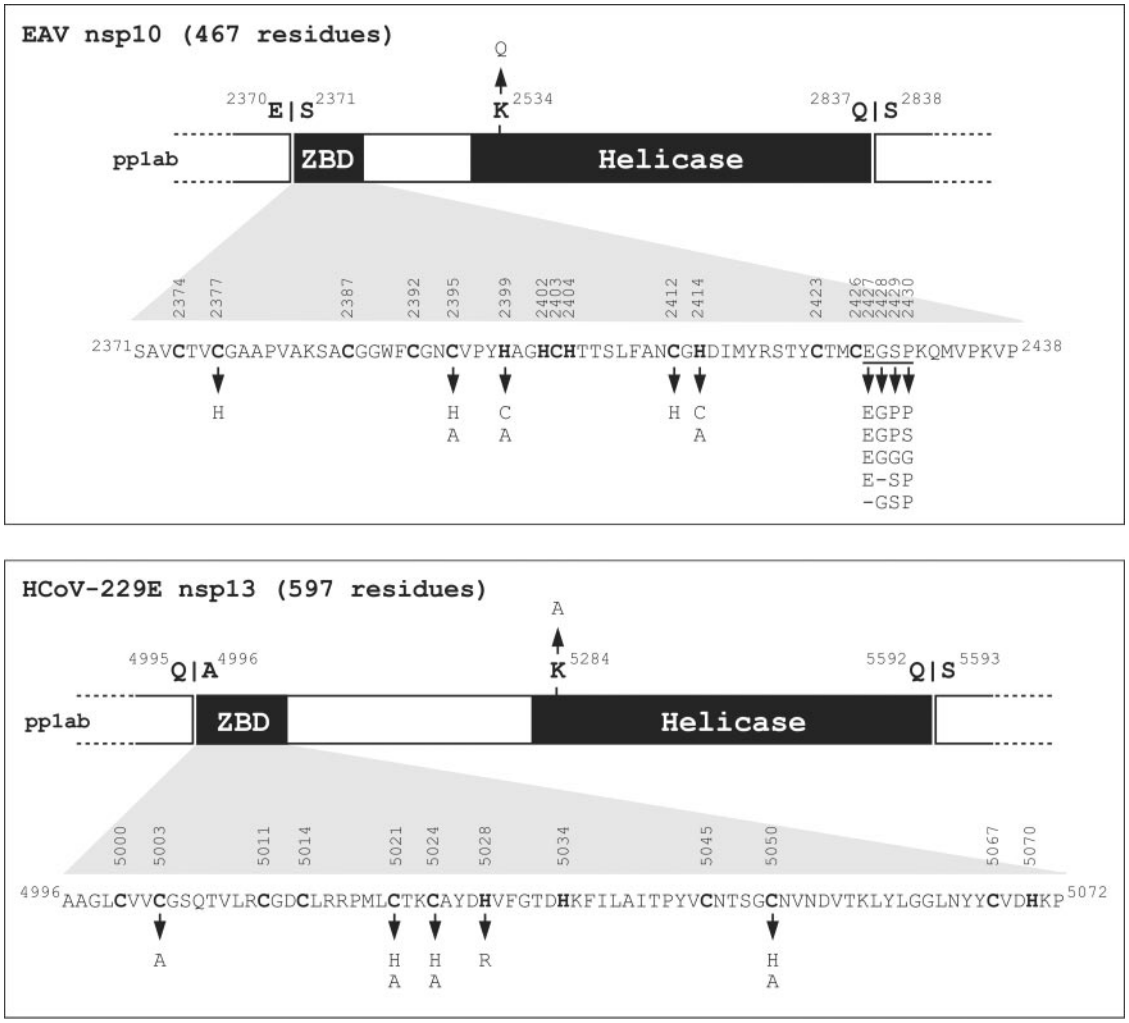

FIG. 1. Sequences of the N-terminal ZBDs associated with the arterivirus EAV nsp10 and coronavirus HCoV-229E nsp13 helicases. Amino acid residues are numbered according to their positions in the pp1ab replicase polyproteins of EAV and HCoV-229E, respectively. 3C-like protease cleavage sites that flank the EAV and HCoV-229E helicases in pp1ab are given, and the hinge spacer region of nsp10 (residues Glu2427 to Pro2430) is underlined. Also indicated are the amino acid substitutions characterized in this study.

was shown that nsp10 and nsp13 share biochemical properties, including nucleic acid-stimulated ATPase and 5′-to-3′ duplex-unwinding (helicase) activities (24, 25). In this study, we focused on the ZBDs of nsp10 and nsp13 to gain insight into the mechanism(s) underlying the diverse defects of EAV mutants carrying substitutions in the nsp10 ZBD (35). To this end, the ATPase and helicase activities of bacterially expressed nsp10 mutants were characterized. In parallel, we expressed and characterized a similar set of HCoV-229E nsp13 mutants which we hoped would allow us to draw more general conclusions about the structure-function relationships of nidovirus helicases.

We found that point mutations in the ZBD have strong position- and substitution-dependent effects on the ATPase and helicase activities of both the coronavirus and arterivirus enzymes. The fact that replacements predicted to retain the potential Zn^{2+}-coordinating activity (Cys for His or His for Cys) proved to be less detrimental than substitution of the same residues with Ala strongly supports the Zn finger function of this domain. In agreement with this interpretation, denaturation-renaturation experiments revealed that, during protein refolding, Zn^{2+} is essential to the restoration of the enzymatic activities of both nsp10 and nsp13. All mutations that inactivated the ATPase and helicase activities of nsp10 blocked EAV genomic RNA and sgRNA synthesis and, consequently, production of virus progeny. In contrast, the in vivo phenotypes of enzymatically active nsp10 mutants varied widely and did not evidently correlate with the levels of the in vitro activities. Collectively, our data imply that the ZBD is involved in nidovirus replication and transcription by controlling the enzymatic activities of the helicase and, possibly, by modulating other, yet-to-be-defined pathway(s).

MATERIALS AND METHODS

Site-directed mutagenesis. A recombination-PCR method (39) was used to introduce point mutations into the helicase-encoding sequences of pMal-nsp13 (previously called pMal-HEL) (9) and pMal-nsp10 (25). Mutations in nsp10 that had already been generated in the full-length EAV cDNA clone (35) were

TABLE 1. Proteins and viruses characterized in this study

Protein or virus	Substitution(s)[b]	Codon in:	
		Wild type	Mutant
Protein[a]			
MBP-EAV nsp10	None (wild type)		
MBP-nsp10_K2534Q	Lys2534→Gln	AAG	CAG
MBP-nsp10_C2377H	Cys2377→His	TGT	CAC
MBP-nsp10_C2395H	Cys2395→His	TGT	CAC
MBP-nsp10_C2395A	Cys2395→Ala	TGT	GCT
MBP-nsp10_H2399C	His2399→Cys	CAC	TGC
MBP-nsp10_H2399A	His2399→Ala	CAC	GCC
MBP-nsp10_C2412H	Cys2412→His	TGC	CAT
MBP-nsp10_H2414C	His2414→Cys	CAC	TGC
MBP-nsp10_H2414A	His2414→Ala	CAC	GCC
MBP-nsp10_S2429P	Ser2429→Pro	TCC	CCC
MBP-nsp10_S2429G/P2430G	Ser2429→Gly and Pro2430→Gly	TCC	GGC
		CCA	GGA
MBP-nsp10_S2429P/P2430S	Ser2429→Pro and Pro2430→Ser	TCC	CCC
		CCA	TCA
MBP-nsp10_ΔE2427	Glu2427 deletion	GAG	
MBP-nsp10_ΔG2428	Gly2428 deletion	GGT	
MBP-HCoV-229E nsp13	None (wild type)		
MBP-nsp13_K5284A	Lys5284→Ala	AAA	GCA
MBP-nsp13_C5003A	Cys5003→Ala	TGT	GCT
MBP-nsp13_C5021H	Cys5021→His	TGC	CAC
MBP-nsp13_C5021A	Cys5021→Ala	TGC	GCC
MBP-nsp13_C5024H	Cys5024→His	TGC	CAC
MBP-nsp13_C5024A	Cys5024→Ala	TGC	GCT
MBP-nsp13_H5028R	His5028→Arg	CAT	CGT
MBP-nsp13_C5050H	Cys5050→His	TGC	CAC
MBP-nsp13_C5050A	Cys5050→Ala	TGC	GCT
Virus[c]			
EAN800	None (wild type)		
EAV_C2395H	Cys2395→His	UGU	CAC
EAV_C2395A	Cys2395→Ala	UGU	GCU
EAV_H2399C	His2399→Cys	CAC	UGC
EAV_H2399A	His2399→Ala	CAC	GCC
EAV_H2414C	His2414→Cys	CAC	UGC
EAV_H2414A	His2414→Ala	CAC	GCC

[a] EAV nsp10 and HCoV-229E nsp13 sequences were expressed as fusions with the *E. coli* MBP.
[b] The numbering of EAV (strain Bucyrus) and HCoV-229E replicase pplab residues is according to GenBank accession numbers X53459 (for EAV) and X69721 (for HCoV-229E).
[c] The infectious EAV clone used in this study, EAN800, is described in Materials and Methods. EAV mutants were derived from EAN800.

transferred to pMal-nsp10 by exchanging suitable DNA fragments. Table 1 summarizes the proteins characterized in this study.

Expression and purification of recombinant proteins. Wild-type and mutant maltose-binding protein (MBP)–HCoV-229E nsp13 and MBP-EAV nsp10 fusion proteins (Table 1) were overexpressed and purified from *Escherichia coli* cells as described previously (9, 25). Aliquots of purified MBP-nsp10 and its mutants were stored at −80°C in buffer A (20 mM Tris-HCl [pH 8.0], 1 M NaCl, 1 mM EDTA, 1 mM EGTA, 0.1% Tween 20, 1 mM dithiothreitol, 10% glycerol). Aliquots of purified MBP-nsp13 and its mutants were stored at −80°C in buffer B (20 mM Tris-HCl [pH 7.5], 200 mM NaCl, 1 mM EDTA, 1 mM dithiothreitol). Protein concentrations of purified fusion proteins were determined by the Lowry assay (14) with bovine serum albumin as a standard.

Denaturation-renaturation experiments. A 1-ml aliquot of purified MBP-nsp10 was mixed with 9 ml of buffer C (20 mM Tris-HCl [pH 8.0], 1 M NaCl, 0.5 mM dithiothreitol, and 10% glycerol) containing 8 M urea. Following incubation at 20°C for 4 h, the protein solution was divided into two 5-ml aliquots. Aliquot I was dialyzed twice against buffer A containing 100 μM zinc acetate, whereas aliquot II was dialyzed twice against buffer A containing 10 mM EDTA. Thereafter, aliquots I and II were extensively dialyzed against buffer A. Likewise, denaturation and renaturation experiments were done with MBP-nsp13. In this case, a 1-ml aliquot of purified MBP-nsp13 was mixed with 9 ml of buffer D (20 mM Tris-HCl [pH 7.5], 200 mM NaCl, 0.5 mM dithiothreitol) containing 8 M urea. The protein solution was incubated at 20°C for 4 h and then divided into two 5-ml aliquots. Aliquot I was dialyzed twice against buffer D containing 100 μM zinc acetate, whereas aliquot II was dialyzed twice against buffer D containing 10 mM EDTA. Finally, both aliquots were dialyzed against buffer B.

ATPase assay. ATPase activity was determined as described previously (24). In all cases, poly(U) was added to the reaction mixtures at a concentration of 150 μg/ml.

Helicase assay. To determine the duplex-unwinding activities, the recombinant proteins were incubated in 40 μl of reaction buffer (20 mM HEPES-KOH [pH 7.4], 5 mM ATP, 10% glycerol, 5 mM magnesium acetate, 2 mM dithiothreitol, 0.1 mg of bovine serum albumin/ml) with 25 fmol of a twin-tailed (forked) DNA substrate, 5′-to-3′ DNA-T30 (24). The NaCl concentration in the reaction mixtures, resulting from substrate and protein storage buffers, was 25 mM. Following incubation for 30 min at 30°C, the reactions were stopped by the addition of 10 μl of 5% sodium dodecyl sulfate (SDS)–15% Ficoll–100 mM EDTA–0.25% bromophenol blue dye. The reaction products were separated on 10 to 20% gradient polyacrylamide–1× Tris-borate-EDTA gels (acrylamide-bisacrylamide, 19 to 1) at 4 W until the bromophenol blue dye approached the bottom of the gel. The gels were exposed to X-ray film at −80°C.

Introduction of nsp10 mutations in EAV full-length cDNA clones. Previously, the effects of mutations on EAV nsp10 function were analyzed by using a derivative of the EAV infectious cDNA clone pEAV030 that contained several synonymous substitutions (35) which were introduced to engineer or remove restriction sites. One of these mutations, which removed a HindIII restriction site (residues 12303 to 12308) close to the 3′ end of the viral cDNA, was later found to affect the fitness of the virus, which became apparent from somewhat delayed

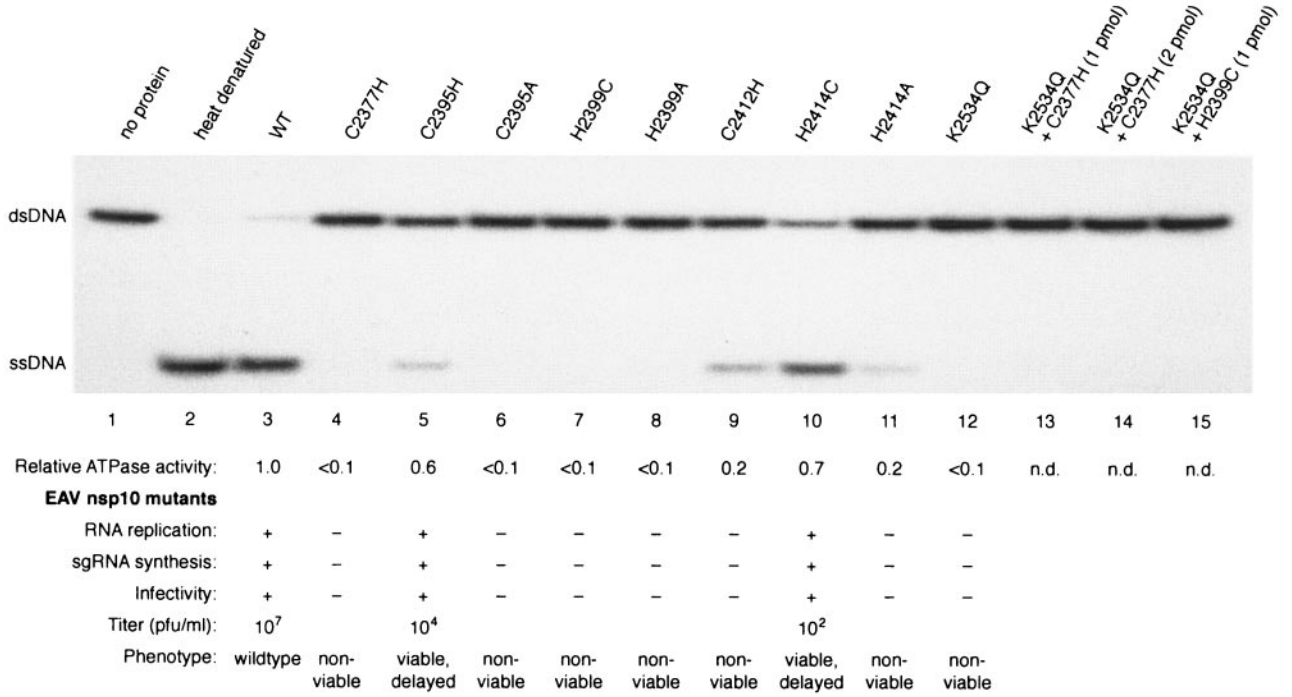

FIG. 2. Effects of substitutions of conserved ZBD Cys and His residues on the enzymatic activities of EAV nsp10 in vitro and on EAV reproduction in BHK-21 cells. Helicase (duplex-unwinding) activities were determined by using a forked DNA substrate containing a 22-bp duplex region and 30-nucleotide, single-stranded oligo(dT) tails (24). This partial-duplex DNA substrate was incubated with 2 pmol (if not indicated otherwise) of purified MBP-nsp10 or its mutant derivatives (for details, see Materials and Methods). Reaction products were analyzed on nondenaturing polyacrylamide gels. Lane 1, incubation without protein; lane 2, heat-denatured substrate; lane 3, MBP-nsp10 (wild type [WT]); lane 4, MBP-nsp10_C2377H; lane 5, MBP-nsp10_C2395H; lane 6, MBP-nsp10_C2395A; lane 7, MBP-nsp10_H2399C; lane 8, MBP-nsp10_H2399A; lane 9, MBP-nsp10_C2412H; lane 10, MBP-nsp10_H2414C; lane 11, MBP-nsp10_H2414A; lane 12, MBP-nsp10_K2534Q; lane 13, 1 pmol of MBP-nsp10_K2534Q and 1 pmol of MBP-nsp10_C2377H; lane 14, MBP-nsp10_K2534Q and MBP-nsp10_C2377H; lane 15, 1 pmol of MBP-nsp10_K2534Q and 1 pmol of MBP-nsp10_H2399C. Below the gel, the relative ATPase activities of the corresponding proteins are given. The activity of the wild-type protein, MBP-nsp10, was taken to be 1.0, and all other ATPase activities were normalized to this value. Also listed are the phenotypes in tissue culture of EAV mutants containing the respective nsp10 ZBD substitutions (Table 1) (35). Titers of progeny virus were determined from tissue culture supernatants harvested at 24 h posttransfection. RNA replication and sgRNA synthesis, respectively, were assessed by immunofluorescence analysis by using antibodies specific for the replicase gene product, nsp3, and the nucleocapsid protein, respectively (for details, see Materials and Methods). RNA synthesis of the EAV mutants, EAV_C2395H and EAV_H2414C, which had delayed growth kinetics, was also studied by Northern blotting (Fig. 3). −, absent; +, present; dsDNA, double-stranded DNA; ssDNA, single-stranded DNA.

virus replication and progeny titers that were about five times lower than those obtained with the original pEAV030 clone. Consequently, novel nsp10 mutations engineered for this study (Table 1) were tested in a novel full-length clone (pEAN800) that lacked this unfavorable 3′-proximal mutation. Virus derived from plasmid pEAN800 was tested extensively and found to be indistinguishable from wild-type virus (data not shown). The previously engineered C2395H, H2399C, and H2414C mutations in nsp10 were also transferred to the pEAN800 backbone to reconfirm the observed phenotypes. Mutations were introduced in an appropriate shuttle vector by standard site-directed PCR mutagenesis as described by Landt et al. (13). After sequence analysis of the complete PCR product, restriction fragments containing the desired mutations were transferred to pEAN800.

RNA transfection, infection, and immunofluorescence analysis. Baby hamster kidney cells (BHK-21; ATCC CCL10) were used for transfection of in vitro-derived RNA transcripts of EAV full-length cDNA clones (34). Infection experiments with EAV were performed on BHK-21 cells essentially as described by de Vries et al. (6). Immunofluorescence analysis with antibodies specific for EAV nsp3 (20) and EAV N (mouse monoclonal antibody 3E2) (15) were performed according to the method of van der Meer et al. (33). Virus titers at 24 h postinfection were determined in plaque assays as described by Snijder et al. (28).

RNA isolation and analysis. Intracellular RNA was isolated by using the acidic phenol method as described by Pasternak et al. (18). RNA was separated in denaturing agarose-formaldehyde gels and detected with ^{32}P-labeled oligonucleotide probe E154 (5′-TTGGTTCCTGGGTGGCTAATAACTACTT-3′), which is complementary to the 3′ end of the EAV genome and recognizes both genomic RNA and sgRNA. Reverse transcription (RT)-PCR experiments were carried out by using E593 (5′-CTGAGCACGGTTTACTGAGTTCAC-3′; EAV nucleotides 8901 to 8924) as the antisense primer for RT and PCR and E156 (5′-GATGAAGACTGGTGGACGG-3′; nucleotides 7220 to 7238) as the sense primer for PCR. The PCR products were sequenced to confirm the presence of the nsp10 mutations.

RESULTS

Selection of ZBD mutations for enzymatic assays. Previously, a large number of EAV mutants with substitutions in the nsp10 ZBD were characterized in tissue culture with an EAV infectious cDNA clone (35). This set of EAV mutants was extended with six novel EAV ZBD mutants (Table 1) which were characterized with respect to genomic RNA and sgRNA synthesis and production of virus progeny. Only two of the six mutants, C2395H and H2414C, proved to be viable, though delayed compared to the wild-type control. In plaque assays, these mutants produced a small-plaque phenotype and strongly reduced virus titers (Fig. 2, bottom panel). The RNA synthesis of the C2395H and H2414C mutants was also char-

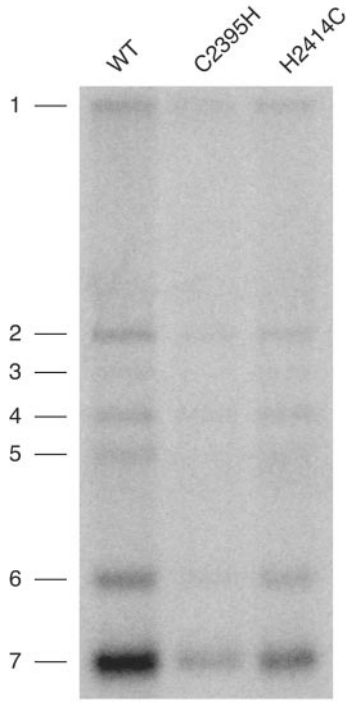

FIG. 3. Hybridization analysis of the RNA synthesis of EAV nsp10 mutants EAV_C2395H and EAV_H2414C. Intracellular RNA was isolated from similar numbers of infected cells at 12 h postinfection. Both genome replication and sgRNA synthesis of the two mutants were reduced compared to a wild-type (WT) control. EAV RNAs 1 to 7 are indicated to the left.

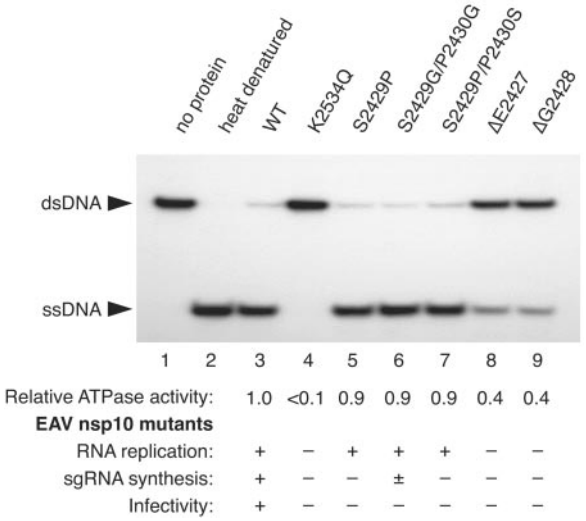

FIG. 4. Effects of substitutions and deletions in the EAV nsp10 hinge spacer region. Helicase activity assays were carried out under the same conditions as in the experiment shown in Fig. 2. Lane 1, reaction without protein; lane 2, heat-denatured substrate; lane 3, MBP-nsp10 (wild type [WT]); lane 4, MBP-nsp10_K2534Q; lane 5, MBP-nsp10_S2429P; lane 6, MBP-nsp10_S2429G/P2430G; lane 7, MBP-nsp10_S2429P/P2430S; lane 8, MBP-nsp10_ΔE2427; lane 9, MBP-nsp10_ΔG2428. Below the gel, the relative ATPase activities of the respective proteins are given. The ATPase activity of the wild-type protein, MBP-nsp10, was taken to be 1.0, and all other activities were normalized to this value. In the bottom panel, the tissue culture phenotypes are given for the EAV mutants containing the respective substitutions or deletions in the hinge spacer region (35). −, absent; +, present; ±, strongly reduced; dsDNA, double-stranded DNA; ssDNA, single-stranded DNA.

acterized by hybridization analysis. RNA derived from wild-type pEAN800 and from both mutant clones was transfected into BHK-21 cells in triplicate, and progeny virus was harvested at complete cytopathic effect. Fresh cells were infected with the three viruses by using a similar multiplicity of infection, and intracellular RNA was isolated at 12 h postinfection, that is, at the end of the first cycle of infection. The presence of the C2395H and H2414C mutations was confirmed by sequence analysis of RT-PCR products. For both mutants, genome replication and sgRNA synthesis could be detected (Fig. 3), but RNA synthesis as a whole was severely reduced compared to the wild-type control, with the reduction being the most severe for the C2395H mutant.

The reverse genetics data obtained in this and a previous study (35) were used to select the most informative ZBD substitutions to be tested in enzymatic assays with bacterially expressed proteins. We decided to characterize mutations that were associated with four different EAV phenotypes (Fig. 2 and 4, bottom panels): (i) no RNA synthesis, (ii) replication of genomic RNA (but no sgRNA synthesis), (iii) genomic RNA and sgRNA synthesis (but no viable virus), and (iv) viable virus but reduced virus titers.

Wild-type and mutant forms of HCoV-229E nsp13 and EAV nsp10 were expressed in *E. coli* as fusion proteins with the MBP and purified by amylose-affinity chromatography. As negative controls, we used Walker A box (38) mutants of nsp10 (MBP-nsp10_K2534Q) and nsp13 (MBP-nsp13_K5284A) (Table 1), which were previously shown to be ATPase deficient (9, 25, 26). SDS-polyacrylamide gel electrophoresis analysis was used to confirm that each of the mutant proteins could be expressed and purified to the same level as the wild-type proteins, MBP-nsp10 and MBP-nsp13 (compare lanes 2 to 15 with lane 1 in Fig. 5A and compare lanes 2 to 9 with lane 1 in Fig. 5B).

Substitutions of conserved ZBD Cys and His residues interfere with ATPase activities of EAV nsp10 and HCoV-229E nsp13. The relative ATPase activities of proteins carrying Cys/His substitutions in the ZBD are presented in the bottom panel of Fig. 2 (for EAV) and in Table 2 (for HCoV-229E). From the 16 Cys/His mutations tested in this study, 8 proteins had a background level of activity and 8 proteins retained significant ATPase activities, which also included one protein, MBP-nsp13_C5024H, whose ATPase activity surpassed that of the wild-type protein. The vast majority of Cys-to-Ala or His-to-Ala mutants was ATPase deficient. Thus, only one of three nsp10 mutants (MBP-nsp10_H2414A) and one of four nsp13 mutants (MBP-nsp13_C5050A) retained significant (albeit reduced) ATPase activities. In striking contrast, the majority of Cys-to-His and His-to-Cys mutants were enzymatically active (Fig. 2 and Table 2). At four positions, nsp10-C2395, nsp10-H2414, nsp13-C5024, and nsp13-C5050, the Ala replacement was more detrimental than the corresponding Cys-to-His or His-to-Cys substitution. At two other positions, nsp10-H2399 and nsp13-C5021, either replacement inactivated the ATPase. Importantly, these effects were observed for both nidovirus

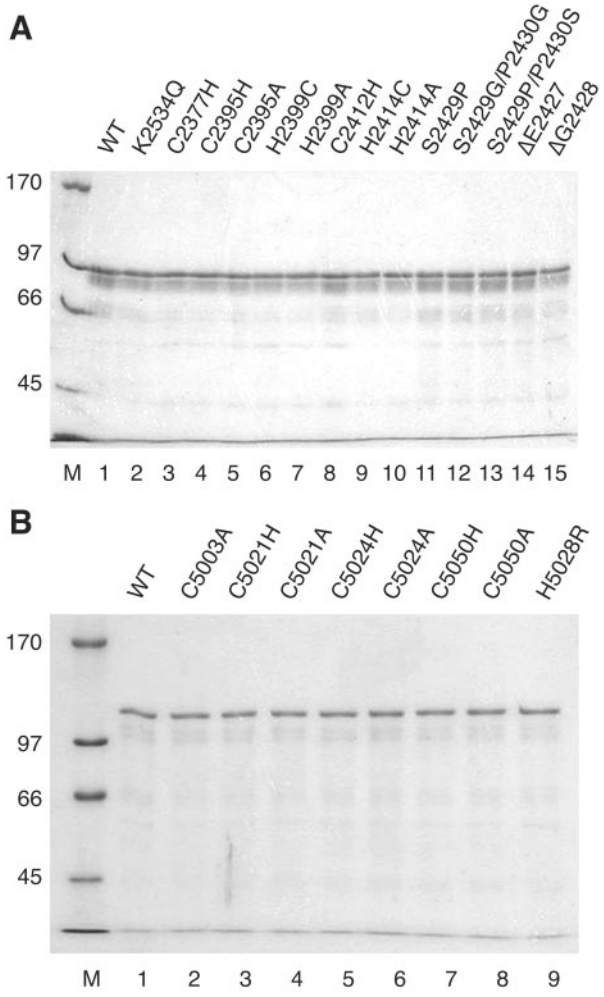

FIG. 5. Purification of bacterially expressed MBP-EAV nsp10 and MBP–HCoV-229E nsp13 fusion proteins. Fusion proteins (1 μg each) were separated by SDS-polyacrylamide gel electrophoresis and stained with Coomassie brilliant blue. Lane M shows the molecular mass markers. (A) MBP-nsp10 fusion proteins. Lane 1, wild-type (WT) MBP-nsp10; lanes 2 to 15, mutant derivatives of MBP-nsp10, with the respective amino acid substitutions indicated above the gel. (B) MBP-nsp13 fusion proteins. Lane 1, MBP-nsp13; lanes 2 to 9, mutant derivatives of MBP-nsp13, with the respective amino acid substitutions indicated above the gel.

homologs. Collectively, these results establish that the ZBD is indispensable for the ATPase activities of nidovirus helicases. Furthermore, the data support, albeit indirectly, the Zn^{2+}-coordinating properties of the conserved Cys and His residues of this domain. The fact that all Cys-to-His and His-to-Cys mutations (including those that gave rise to replication-competent viruses) affected the ATPase activities of nidovirus helicases suggests that the interplay between the zinc-binding and catalytic domains is finely tuned.

Duplex-unwinding activity of nsp10 is sensitive to substitutions of conserved ZBD Cys and His residues. As previously reported, nidovirus helicases have 5′-to-3′ duplex-unwinding activities that depend on ATP hydrolysis (24, 25, 32). We therefore sought to investigate whether (and to what extent) reduced ATPase activities would affect the duplex-unwinding

TABLE 2. Relative ATPase activities of MBP–HCoV-229E nsp13 fusion proteins carrying substitutions in the ZBD

Protein	Relative ATPase activity[a]
MBP-nsp13	1.0
MBP-nsp13_K5284A	<0.1
MBP-nsp13_C5003A	<0.1
MBP-nsp13_C5021H	<0.1
MBP-nsp13_C5021A	<0.1
MBP-nsp13_C5024H	1.5
MBP-nsp13_C5024A	<0.1
MBP-nsp13_H5028R	0.2
MBP-nsp13_C5050H	0.9
MBP-nsp13_C5050A	0.6

[a] The ATPase activity of the wild-type protein, MBP-nsp13, was taken to be 1.0, and all other activities were normalized to this value. The Walker A box-substituted protein, MBP-nsp13_K5284A, was used as a negative control. Each value represents the average of the results from three independent determinations, which did not vary by more than 15%.

activities of the ZBD mutants. As shown for MBP-nsp10 in Fig. 2, there was a clear link between the ATPase and unwinding activities of a given protein. As expected, mutants that lacked ATPase activity also lacked helicase activity (compare lanes 4, 6, 7, and 8 with lane 3). However, the helicase and ATPase activities were not equally affected by a given mutation in all proteins. Such a discrepancy between the observed ATPase and helicase activities was particularly evident in the nsp10_C2395H mutant that, despite considerable ATPase activity (60% of the wild-type activity), only had a poor helicase activity compared to other mutants with similar (H2414C) or even much less ATPase activity (C2412H) (compare lanes 5 with lanes 9 and 10 in Fig. 2). It thus appears that the C2395H mutation inhibits the helicase activity through both ATPase-dependent and -independent pathways. Taken together, the results suggest that ZBD controls the activities of the catalytic domain and indicate that this function may involve ATPase-dependent and -independent determinants.

Zn^{2+} is an essential structural cofactor for coronavirus and arterivirus helicases. The observed strong effects of single ZBD mutations on the enzymatic activities of the catalytic domain strongly suggest that major conformational changes in the ZBD will disrupt the activities of the downstream helicase. Hence, the enzymatic activities of HCoV-229E nsp13 and EAV nsp10 should also be extremely sensitive to Zn^{2+} depletion. To test this hypothesis, purified MBP-nsp13 and MBP-nsp10 were denatured in urea-containing buffer and subsequently renatured in buffer containing either 100 μM zinc acetate or 10 mM EDTA (see Materials and Methods for details). Subsequent ATPase activity assays consistently revealed that proteins refolded in Zn^{2+}-containing buffer had regained ATPase activity, whereas no significant activity was found for proteins refolded in Zn^{2+}-free buffer (Fig. 6). The latter proteins could not be reactivated by supplementing the ATPase reaction buffer with zinc acetate (data not shown). Similar results were obtained in the helicase assay (data not shown). The data lead us to suggest that Zn^{2+} is an essential structural (rather than catalytic) cofactor of nidovirus helicases which, most probably, is required to maintain the enzymatically active conformation. In line with this interpretation, helicase

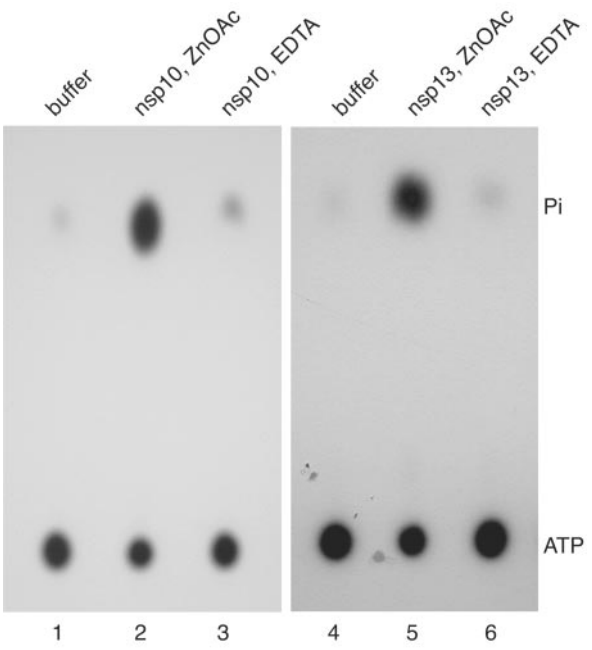

FIG. 6. Zn^{2+} is an essential structural cofactor for the ATPase activities of arterivirus EAV nsp10 and coronavirus HCoV-229E nsp13. MBP-nsp10 and MBP-nsp13 were denatured in urea-containing buffer and subsequently renatured in buffer containing zinc acetate and EDTA, respectively. The ATPase activities of the renatured MBP-nsp10 (lanes 2 and 3) and MBP-nsp13 (lanes 5 and 6) fusion proteins were analyzed by the [γ-^{32}P]ATP thin-layer chromatography assay described in Materials and Methods. ATPase reactions were done with buffer alone (lanes 1 and 4), with proteins renatured in the presence of 100 μM zinc acetate (ZnOAc, lanes 2 and 5), and with proteins renatured in the presence of 10 mM EDTA (lanes 3 and 6). The positions of ATP and P_i are indicated.

sequence alignments revealed that the ZBD is the only domain in which residues with known zinc-binding potential (Cys, His, and Glu) (35) are conserved among arteriviruses and coronaviruses (data not shown). These results are fully consistent with the genetic and biochemical data presented above and provide further evidence for a control function of the ZBD over the catalytic domain.

ZBD may provide an essential *cis*-acting function for the EAV helicase. To address the mechanism by which the ZBD controls the activities of the catalytic domain, the unwinding activities of two nsp10 derivatives with ZBD deletions were tested. Both proteins proved to be enzymatically inactive and could not be rescued by a separate ZBD provided in *trans* (data not shown). The helicase activity was also not rescued by intra-allele complementation in an assay with a mixture of two inactive mutants with replacements in either the catalytic domain (the Walker A box mutant protein, MBP-nsp10_K2534Q) or the ZBD (MBP-nsp10_C2377H or MBP-nsp10_H2399C) (Fig. 2, lanes 13 to 15). Although the negative outcome of these experiments may be explained in numerous ways, the results, combined with the helicase activity of the intact nsp10, indicate that the nsp10 enzymatic activity is critically dependent upon ZBD functions provided in *cis*.

Enzymatic activities of ZBD hinge spacer mutants. In addition to mutations in the ZBD itself, we characterized the enzymatic activities of a series of hinge spacer mutations that were proven by reverse genetics to block viral reproduction in tissue culture (35). MBP-nsp10 derivatives with single (MBP-nsp10_S2429P) or double substitutions (MBP-nsp10_S2429G/P2430G and MBP-nsp10_S2429P/P2430S) had almost wild-type ATPase activities, whereas single-amino-acid deletions in this region (MBP-nsp10_ΔE2427 and MBP-nsp10_ΔG2428) led to reduced (but still significant) ATPase activities (Fig. 4). The unwinding and ATPase activities of these mutant proteins were affected to similar extents (compare the data in the top and bottom panels of Fig. 4), indicating that the hinge region may control the nsp10 helicase activity by modulating the associated ATPase activity.

Complex relationship between effects of EAV ZBD mutations on in vitro enzymatic activities and virus phenotype. As could be expected from the pivotal role of the helicase for EAV reproduction (35), mutations that inactivated the enzymatic activities of nsp10 also completely blocked sgRNA and genomic RNA synthesis and production of infectious progeny when tested in the EAV infectious clone (Fig. 2, lanes 4, 6 to 8, and 12, and Fig. 4, lane 4). This nonviable phenotype was also seen in 4 other mutants for which low ATPase/helicase activities had been measured in vitro (Fig. 2, lanes 9 and 11, and Fig. 4, lanes 8 and 9). In contrast, all five mutants with ATPase activities of $\geq$60% of the wild-type level proved to be replication competent, irrespective of the level of their helicase activities and also irrespective of whether the mutation was located in the ZBD or the hinge spacer region. Three of these mutations (with substitutions in the hinge spacer) showed almost wild-type ATPase/helicase activities in vitro but, in the infectious clone, caused severe defects in viral sgRNA synthesis (Fig. 4, lanes 5 to 7). Only two of the ZBD mutations were compatible with virus reproduction. Remarkably, one of these mutations was C2395H, a protein with very weak helicase activity compared to other enzymatically active nsp10 mutants (Fig. 2, lanes 5 and 9 to 11). This comparative analysis shows that, for most mutations, there is no simple correlation between the virus phenotype in tissue culture and the enzymatic activities of the catalytic domain measured in vitro. In our experiments, partial defects in the nsp10 ATPase activity turned out to be more critical to EAV replication than a reduced helicase activity. Furthermore, our data indicate that, besides its involvement in the ATPase/helicase activities, the ZBD-associated hinge spacer may control another yet-to-be identified activity that is required for nidovirus sgRNA synthesis.

DISCUSSION

In this study, we provide several lines of evidence to support a zinc-binding activity of the nidovirus-specific ZBD. Furthermore, the ZBD is shown to be of critical importance to the ATPase and duplex-unwinding activities of the C-proximal helicase domain. The observed dependence of the catalytic domain on the N-terminal ZBD seems to be one of the mechanisms by which the ZBD controls key processes of arterivirus (and probably coronavirus) RNA synthesis.

Zn fingers contain conserved Cys and His residues and have been implicated in diverse functions, including protein-protein interactions as well as binding of single- and double-stranded

nucleic acids (12). The fusion of a Zn finger and a helicase domain in a single protein has been identified in a growing number of helicases (1, 17, 37). However, to date, there are only few examples where this structural association was probed experimentally in functional assays. Similar to our data, Poplawski et al. (21) showed recently that a mutation in the ZBD of an archaeal minichromosome maintenance protein, belonging to a protein family that most probably constitutes the eukaryotic replicative helicase, impaired the DNA-binding, ATPase, and unwinding activities of the enzyme, indicating interactions between the Zn finger and enzymatic domains. For RNA viruses, the association of Zn finger and helicase domains in a single protein has only been reported for the order *Nidovirales.* We have shown here that Zn^{2+} is an indispensable structural component of arterivirus and coronavirus helicases. Our mutagenesis data also indicate that the structures of nidovirus ZBDs are highly constrained and that there is extensive communication between the ZBD and helicase domains. Thus, even substitutions expected to preserve the zinc-binding properties of the domain (Cys→His or His→Cys) significantly reduced and, in some cases, completely abolished the ATPase and unwinding activities of the C-terminal helicase domain.

Using EAV reverse genetics, it has been shown in this and a previous study (35) that most replacements of conserved nsp10 ZBD Cys/His residues result in a complete block of viral RNA synthesis. These in vivo data were now complemented by assessing the enzymatic properties of the ZBD mutants in vitro. We found that, without exception, nondetectable ATPase and helicase activities in vitro correlate with nonviable phenotypes in vivo. However, we also observed that some mutations produced nonviable phenotypes (nsp10_C2412H and nsp10_H2414A), although the proteins possessed significant ATPase and helicase activities. Collectively, the data support the idea that EAV reproduction is most sensitive to the level of nsp10 ATPase activity. Further studies are needed to elucidate the exact mechanism of this dependence.

A potential functional parallel may exist between the nidovirus ZBD/helicase and herpes simplex virus type 1 UL5/UL52, a heteromeric protein complex with zinc-binding and helicase domains. These domains reside in separate proteins that are both necessary for ATPase and unwinding activities (2). Like in our experiments, mutations in the Zn finger of the herpes simplex virus type 1 UL5 protein were shown to affect the enzymatic activities of the associated UL52 helicase (2). We therefore sought to reconstitute a functional nidovirus helicase from separately expressed Zn finger and helicase domains. The inability to reconstitute nidovirus helicase activity by separate expression of the ZBD and the helicase region may be due to purely technical reasons (for example, incorrectly selected domain borders of the zinc-binding and helicase domains). Alternatively, and in our opinion much more likely, nidoviruses may have evolved a helicase whose activities strictly depend on a ZBD to which the catalytic domain remains covalently bound throughout the infection cycle.

The zinc-binding and helicase core domains of nsp10 are thought to be connected by a so-called hinge spacer segment (35). Previously, point mutations in this region were found to selectively disrupt EAV sgRNA synthesis (34, 35). Interestingly, the corresponding proteins with single or double amino acid substitutions in this region (nsp10_S2429P, nsp10_S2429G/P2430G, and nsp10_S2429P/P2430S) were found to exhibit nearly wild-type ATPase and helicase activities, suggesting that nsp10 has yet another role in sgRNA synthesis that cannot be assessed by the existing in vitro assays. Further studies are needed to determine whether interactions with specific RNA substrates and/or other proteins of the viral replication complex are affected in these mutants. In contrast to amino acid replacements, deletions of single residues in the same region (nsp10_ΔE2427 and nsp10_ΔG2428) considerably reduced both ATPase and helicase activities in vitro, which is consistent with the previously observed disruption of both genomic RNA and sgRNA synthesis in tissue culture (35). It remains to be determined whether the reduction of the enzymatic activities of nsp10 is the sole cause of the nonviable phenotype of these mutants or whether other mechanisms are also involved. Although we do not know precisely how these deletions exert their deleterious effects, our results illustrate that the integrity of the viral helicase, even in the variable region connecting the Zn finger and catalytic domains, is extremely important for the viability of nidoviruses.

Finally, our comparative analysis of EAV and HCoV-229E helicases identified nsp13 mutants which look most promising for a future characterization in vivo. The data lead us to predict that the nsp13 mutants C5024H, C5050H, and C5050A with relative ATPase activities of ≥0.6 will support HCoV-229E RNA synthesis and, possibly, also virus production. A further detailed characterization of these mutants in vitro and in vivo should be most insightful for the dissection of the precise role(s) that nsp13 plays in coronavirus reproduction. It has been argued that, because of the vital role of its enzymatic activities for viral replication, nsp13 may represent a suitable target for antiviral therapy of coronavirus infections including severe acute respiratory syndrome (4, 10, 32). However, given the huge number of cellular helicases, the development of selective coronavirus (nidovirus) helicase inhibitors can be expected to be a major challenge. In this respect, the essential and severely constrained interaction between the enzymatic and zinc-binding domains of nidovirus helicases identified in this study may offer a novel target for the development of highly selective antinidoviral drugs.

ACKNOWLEDGMENT

This work was supported by grants from the Deutsche Forschungsgemeinschaft awarded to J.Z. (ZI 618/2, SFB 479 TP A8).

REFERENCES

1. **Aubry, F., M. G. Mattei, and F. Galibert.** 1998. Identification of a human 17p-located cDNA encoding a protein of the Snf2-like helicase family. Eur. J. Biochem. **254:**558–564.
2. **Biswas, N., and S. K. Weller.** 1999. A mutation in the C-terminal putative Zn2+ finger motif of UL52 severely affects the biochemical activities of the HSV-1 helicase-primase subcomplex. J. Biol. Chem. **274:**8068–8076.
3. **Brierley, I., P. Digard, and S. C. Inglis.** 1989. Characterization of an efficient coronavirus ribosomal frameshifting signal: requirement for an RNA pseudoknot. Cell **57:**537–547.
4. **Davidson, A., and S. Siddell.** 2003. Potential for antiviral treatment of severe acute respiratory syndrome. Curr. Opin. Infect. Dis. **16:**565–571.
5. **den Boon, J. A., E. J. Snijder, E. D. Chirnside, A. A. de Vries, M. C. Horzinek, and W. J. Spaan.** 1991. Equine arteritis virus is not a togavirus but belongs to the coronaviruslike superfamily. J. Virol. **65:**2910–2920.
6. **de Vries, A. A., E. D. Chirnside, P. J. Bredenbeek, L. A. Gravestein, M. C. Horzinek, and W. J. Spaan.** 1990. All subgenomic mRNAs of equine arteritis virus contain a common leader sequence. Nucleic Acids Res. **18:**3241–3247.
7. **Gorbalenya, A. E.** 2001. Big nidovirus genome. When count and order of domains matter. Adv. Exp. Med. Biol. **494:**1–17.

8. **Gorbalenya, A. E., E. V. Koonin, A. P. Donchenko, and V. M. Blinov.** 1989. Coronavirus genome: prediction of putative functional domains in the nonstructural polyprotein by comparative amino acid sequence analysis. Nucleic Acids Res. **17:**4847–4861.
9. **Heusipp, G., U. Harms, S. G. Siddell, and J. Ziebuhr.** 1997. Identification of an ATPase activity associated with a 71-kilodalton polypeptide encoded in gene 1 of the human coronavirus 229E. J. Virol. **71:**5631–5634.
10. **Ivanov, K. A., V. Thiel, J. C. Dobbe, Y. van der Meer, E. J. Snijder, and J. Ziebuhr.** 2004. Multiple enzymatic activities associated with severe acute respiratory syndrome coronavirus helicase. J. Virol. **78:**5619–5632.
11. **Lai, M. M. C., and K. V. Holmes.** 2001. *Coronaviridae*: the viruses and their replication, p. 1163–1185. *In* D. M. Knipe and P. M. Howley (ed.), Fields virology, 4th ed., vol. 1. Lippincott Williams & Wilkins, Philadelphia, Pa.
12. **Laity, J. H., B. M. Lee, and P. E. Wright.** 2001. Zinc finger proteins: new insights into structural and functional diversity. Curr. Opin. Struct. Biol. **11:**39–46.
13. **Landt, O., H. P. Grunert, and U. Hahn.** 1990. A general method for rapid site-directed mutagenesis using the polymerase chain reaction. Gene **96:**125–128.
14. **Lowry, O. H., N. J. Rosebrough, A. L. Farr, and R. J. Randall.** 1951. Protein measurement with the Folin phenol reagent. J. Biol. Chem. **193:**265–275.
15. **MacLachlan, N. J., U. B. Balasuriya, J. F. Hedges, T. M. Schweidler, W. H. McCollum, P. J. Timoney, P. J. Hullinger, and J. F. Patton.** 1998. Serologic response of horses to the structural proteins of equine arteritis virus. J. Vet. Diagn. Investig. **10:**229–236.
16. **Molenkamp, R., H. van Tol, B. C. Rozier, Y. van der Meer, W. J. Spaan, and E. J. Snijder.** 2000. The arterivirus replicase is the only viral protein required for genome replication and subgenomic mRNA transcription. J. Gen. Virol. **81:**2491–2496.
17. **Nakagawa, T., and H. Ogawa.** 1999. The Saccharomyces cerevisiae MER3 gene, encoding a novel helicase-like protein, is required for crossover control in meiosis. EMBO J. **18:**5714–5723.
18. **Pasternak, A. O., A. P. Gultyaev, W. J. Spaan, and E. J. Snijder.** 2000. Genetic manipulation of arterivirus alternative mRNA leader-body junction sites reveals tight regulation of structural protein expression. J. Virol. **74:**11642–11653.
19. **Pasternak, A. O., E. van den Born, W. J. Spaan, and E. J. Snijder.** 2001. Sequence requirements for RNA strand transfer during nidovirus discontinuous subgenomic RNA synthesis. EMBO J. **20:**7220–7228.
20. **Pedersen, K. W., Y. van der Meer, N. Roos, and E. J. Snijder.** 1999. Open reading frame 1a-encoded subunits of the arterivirus replicase induce endoplasmic reticulum-derived double-membrane vesicles which carry the viral replication complex. J. Virol. **73:**2016–2026.
21. **Poplawski, A., B. Grabowski, S. E. Long, and Z. Kelman.** 2001. The zinc finger domain of the archaeal minichromosome maintenance protein is required for helicase activity. J. Biol. Chem. **276:**49371–49377.
22. **Sawicki, S. G., and D. L. Sawicki.** 1995. Coronaviruses use discontinuous extension for synthesis of subgenome-length negative strands. Adv. Exp. Med. Biol. **380:**499–506.
23. **Sawicki, S. G., and D. L. Sawicki.** 1998. A new model for coronavirus transcription. Adv. Exp. Med. Biol. **440:**215–219.
24. **Seybert, A., A. Hegyi, S. G. Siddell, and J. Ziebuhr.** 2000. The human coronavirus 229E superfamily 1 helicase has RNA and DNA duplex-unwinding activities with 5′-to-3′ polarity. RNA **6:**1056–1068.
25. **Seybert, A., L. C. van Dinten, E. J. Snijder, and J. Ziebuhr.** 2000. Biochemical characterization of the equine arteritis virus helicase suggests a close functional relationship between arterivirus and coronavirus helicases. J. Virol. **74:**9586–9593.
26. **Seybert, A., and J. Ziebuhr.** 2001. Guanosine triphosphatase activity of the human coronavirus helicase. Adv. Exp. Med. Biol. **494:**255–260.
27. **Snijder, E. J., P. J. Bredenbeek, J. C. Dobbe, V. Thiel, J. Ziebuhr, L. L. Poon, Y. Guan, M. Rozanov, W. J. Spaan, and A. E. Gorbalenya.** 2003. Unique and conserved features of genome and proteome of SARS-coronavirus, an early split-off from the coronavirus group 2 lineage. J. Mol. Biol. **331:**991–1004.
28. **Snijder, E. J., J. C. Dobbe, and W. J. Spaan.** 2003. Heterodimerization of the two major envelope proteins is essential for arterivirus infectivity. J. Virol. **77:**97–104.
29. **Snijder, E. J., and M. C. Horzinek.** 1993. Toroviruses: replication, evolution and comparison with other members of the coronavirus-like superfamily. J. Gen. Virol. **74:**2305–2316.
30. **Snijder, E. J., and J. J. M. Meulenberg.** 2001. Arteriviruses, p. 1205–1220. *In* D. M. Knipe and P. M. Howley (ed.), Fields virology, 4th ed., vol. 1. Lippincott Williams & Wilkins, Philadelphia, Pa.
31. **Thiel, V., J. Herold, B. Schelle, and S. G. Siddell.** 2001. Viral replicase gene products suffice for coronavirus discontinuous transcription. J. Virol. **75:**6676–6681.
32. **Thiel, V., K. A. Ivanov, Á. Putics, T. Hertzig, B. Schelle, S. Bayer, B. Weißbrich, E. J. Snijder, H. Rabenau, H. W. Doerr, A. E. Gorbalenya, and J. Ziebuhr.** 2003. Mechanisms and enzymes involved in SARS coronavirus genome expression. J. Gen. Virol. **84:**2305–2315.
33. **van der Meer, Y., H. van Tol, J. Krijnse Locker, and E. J. Snijder.** 1998. ORF1a-encoded replicase subunits are involved in the membrane association of the arterivirus replication complex. J. Virol. **72:**6689–6698.
34. **van Dinten, L. C., J. A. den Boon, A. L. Wassenaar, W. J. Spaan, and E. J. Snijder.** 1997. An infectious arterivirus cDNA clone: identification of a replicase point mutation that abolishes discontinuous mRNA transcription. Proc. Natl. Acad. Sci. USA **94:**991–996.
35. **van Dinten, L. C., H. van Tol, A. E. Gorbalenya, and E. J. Snijder.** 2000. The predicted metal-binding region of the arterivirus helicase protein is involved in subgenomic mRNA synthesis, genome replication, and virion biogenesis. J. Virol. **74:**5213–5223.
36. **van Dinten, L. C., A. L. Wassenaar, A. E. Gorbalenya, W. J. Spaan, and E. J. Snijder.** 1996. Processing of the equine arteritis virus replicase ORF1b protein: identification of cleavage products containing the putative viral polymerase and helicase domains. J. Virol. **70:**6625–6633.
37. **Villard, L., A. M. Lossi, C. Cardoso, V. Proud, P. Chiaroni, L. Colleaux, C. Schwartz, and M. Fontes.** 1997. Determination of the genomic structure of the XNP/ATRX gene encoding a potential zinc finger helicase. Genomics **43:**149–155.
38. **Walker, J. E., M. Saraste, M. J. Runswick, and N. J. Gay.** 1982. Distantly related sequences in the alpha- and beta-subunits of ATP synthase, myosin, kinases and other ATP-requiring enzymes and a common nucleotide binding fold. EMBO J. **1:**945–951.
39. **Yao, Z., D. H. Jones, and C. Grose.** 1992. Site-directed mutagenesis of herpesvirus glycoprotein phosphorylation sites by recombination polymerase chain reaction. PCR Methods Appl. **1:**205–207.
40. **Ziebuhr, J.** 2005. The coronavirus replicase. Curr. Top. Microbiol. Immunol. **287:**57–94.
41. **Ziebuhr, J.** 2004. Molecular biology of severe acute respiratory syndrome coronavirus. Curr. Opin. Microbiol. **7:**412–419.
42. **Ziebuhr, J., E. J. Snijder, and A. E. Gorbalenya.** 2000. Virus-encoded proteinases and proteolytic processing in the Nidovirales. J. Gen. Virol. **81:**853–879.
43. **Zúñiga, S., I. Sola, S. Alonso, and L. Enjuanes.** 2004. Sequence motifs involved in the regulation of discontinuous coronavirus subgenomic RNA synthesis. J. Virol. **78:**980–994.